Review

Fast pyrolysis oil stabilization kinetics over a Ni-Cu catalyst using propionic acid as a model compound

Daria Otyuskaya[a], Joris W. Thybaut[a], Vaios Alexiadis[a], Maria Alekseeva[b], Robbie Venderbosch[c], Vadim Yakovlev[b], Guy B. Marin[a]

[a] Ghent University, Laboratory for Chemical Technology, Technologiepark 914, Ghent, B-9052, Belgium
[b] Boreskov Institute of Catalysis, 5, pr. Akad. Lavrentieva, 630090, Novosibirsk, Russia
[c] Biomass Technology Group BV, Josink Esweg 34, 7545 PN, Enschede, The Netherlands

A B S T R A C T

Propionic acid hydrotreatment was investigated as a model reaction for fast pyrolysis oil stabilization over a Ni-Cu/SiO$_2$-ZrO$_2$ catalyst. Intrinsic kinetics were acquired within a wide range of operating conditions resulting in an extended dataset of 37 experiments. Two major Ni-catalyzed conversion pathways, being hydrogenation to propanol and decarbonylation into ethane and carbon monoxide, were identified. Propanol, formed on the Ni sites after a series of hydrogenation steps, was found to also undergo decarbonylation at the investigated operating conditions. Additionally, the metal oxide support, catalyzed the esterification between propionic acid and propanol. The observation of only traces of decarboxylation and ketonization products indicated that these conversion pathways were not particularly pronounced in the investigated range of operating conditions. Due to the experimentally observed high methanation activity of Ni-Cu/SiO$_2$-ZrO$_2$, the hydrogenation route, which was favored at lower temperatures and higher total and partial hydrogen pressure was determined to be the preffered conversion pathway as compared to the decarbonylation route. The acquired experimental dataset was utilized for the construction of a comprehensive hydrodeoxigenation kinetic model based on elementary steps. The first step, which is a joint one in the decarbonylation and hydrogenation route, was found to be rate determining with activation energy of 118 kJ mol^{-1}. The higher selectivity to propyl propionate compared to propane was ascribed to the higher affinity of propanol for the metal oxide support than for metal active sites.

1. Introduction

With the continued steady growth in the world population and living standards during this early twenty first century, there is a significant increase in consumption of non-renewable natural resources, e.g., gas, petroleum and coal [1,2]. Together with geopolitical and environmental concerns, such as global warming and CO$_2$ emissions, this has boosted the search for alternative, economically viable, environmentally friendly and energy efficient processes for renewable fuels production. In that light, ligno-cellulosic biomass conversion appears as a very promising and attractive way to fulfill energy demands while keeping the emissions under control [3].

At present, one of the most well developed technologies for ligno-cellulosic biomass processing is fast pyrolysis. Despite the high yield and quality compared to bio oils provided by alternative conversion technologies [4–6], fast pyrolysis oil still cannot be used directly as a transportation fuel due to its acidity, limited energy density and issues with long term stability [7,8]. Challenges in direct fast pyrolysis utilization are associated with the high content of oxygenated organic compounds with a high degree of functionalization. Among numerous technologies proposed for oxygen removal from the fast pyrolysis oil,

catalytic hydrotreatment, commonly referred to as hydrodeoxygenation (HDO), is the most widely investigated [9–11].

The ultimate goal of the fast pyrolysis oil upgrading via HDO is to increase the effective H/C ratio which consequently increases its energy content and to decrease the O/C ratio to eliminate the oxygen heteroatom. Full, or deep HDO allows reaching the desired results but requires rather severe reaction conditions and excessive hydrogen consumption, resulting in increased investment and operational costs [7,12–14]. Hence, an alternative strategy of 'stabilization', involving milder HDO conditions and only partial oxygen content removal while simultaneously avoiding excessive hydrogen addition, can be employed. The obtained product still contains traces of oxygen, yet the number of oxygen functionalities is limited to such an extent that it no longer exhibits the above-mentioned drawbacks characteristic for fast pyrolysis oil. As a result, direct usage of the stabilized oil, or at least co-processing in existing crude oil refineries, comes within reach.

The reactions occurring during catalytic HDO can follow different oxygen-removal routes: during hydrodeoxygenation oxygen is removed in the form of water, whereas decarbonylation and decarboxylation eliminates oxygen from the bio oil as CO and CO$_2$, respectively. From the hydrogen consumption perspective, the facilitation of decarbon(x)

ylation reactions is beneficial since one or two oxygen atoms are removed at the expense of one carbon atom with limited, if any, hydrogen consumption [15–17]. Hydrodeoxygenation reactions allow to eliminate oxygen while retaining carbon and, therefore, improve carbon utilization, but inevitably lead to higher hydrogen consumption [7,14,15]. It is, hence, essential to identify an adequate ratio between the occurrence of the above-mentioned reactions to develop efficient and commercially competitive process.

Another challenge associated with fast pyrolysis oil HDO, either being performed at mild or deep HDO conditions, is the catalyst selection. The strong resemblance of fast pyrolysis oil hydrotreatment with conventional crude oil hytrotreatment seems to suggest the use of conventional hydroprocessing catalysts as applied in the petrochemical industry for crude oil hydrodesulphurisation and hydrodenitrogenation. However, when used for fast pyrolysis oil hydrotreatment, their activity rapidly declines not only due to the lack of sulphur in the fast pyrolysis oil, resulting in sulphur depletion from the catalyst and hence, activity losses, but more likely because of coke deposits, contamination with liquids constituent and active metal leaching [18–22]. Therefore, alternative materials are being investigated for fast pyrolysis oil hydrotreatment, including noble metals. This group of catalysts, even though exhibiting promising results, has the major disadvantages of excessive price and limited availability, which would render the process economically non-feasible [8,23]. To tackle this issue, various non-noble transition metals have recently been employed for bio oil HDO, among which Ni-based catalysts, that have exhibited excellent activity and selectivity towards targeted reactions, e.g., hydrogenation and decarbon(x)ylation [8,23–26].

The key points for the development of an efficient fast pyrolysis oil HDO process include, apart from the design of novel catalytic materials, the reactor technology optimization and fine tuning of the operating conditions. A proper understanding of the reaction kinetics is of significant benefit for both of the stated issues. A kinetic model is not only an essential component of every reactor technology development and process optimization but it is also highly beneficial in the reaction mechanism elucidation and catalyst property optimization [27,28].

The goal of the present work is, hence, to experimentally measure the reaction kinetics and to develop a kinetic model for fast pyrolysis oil stabilization with propionic acid as a model compound. Due to the high chemical complexity of fast pyrolysis oil, it is a common practice to use such a model compound at laboratory scale. Being a carboxylic acid, propionic acid also provides the necessary information on the ratio between hydrogenation and decarbon(x)ylation activity, which is an essential feature for hydrogen consumption assessment. A high metal loading Ni-Cu based catalyst, recently developed by Yakovlev et.al. [29–32], was selected for the HDO measurements. These catalytic systems have been already benchmarked against several noble metal catalysts and exhibited remarkable performance in fast pyrolysis oil HDO featuring low coke formation, high stability and low yields of undesired reaction products [20,32,33]. The present work focuses on quantification of Ni-Cu/SiO$_2$-ZrO$_2$ catalyst performance in terms of catalytic and kinetic descriptors.

2. Procedures

2.1. Catalyst and materials

Propionic acid (99%) was supplied by Alfa Aesar. n-Hexane (95 + %) and n-octane (99 + %) were purchased from Acro Organics. 99.9% nitrogen and hydrogen were obtained from Air Liquide. A 46 wt%Ni-5 wt %Cu/SiO$_2$-ZrO$_2$ bimetallic catalyst was prepared by sol-gel synthesis according to the procedure reported elsewhere [30,31]. The detailed characterization of the investigated catalyst including its TPR profile, textural properties and specific surface area of the active component, elemental composition of the catalyst surface, XRD patterns and HRTEM images, have been previously reported by Heeres et. al. [33].

The obtained catalyst powder was pressed into flakes and subsequently crushed into pellets of 300–500 μm diameter, allowing intrinsic kinetics determination, i.e., there was a negligible impact of mass transport and pressure drop on the overall performance.

2.2. Intrinsic kinetic measurements of propionic acid HDO

All the propionic acid HDO experiments were performed in a high-throughput kinetic mechanistic investigation setup [34,35]. The liquid feed comprising propionic acid together with n-hexane and n-octane used as solvent and internal standard respectively is introduced via a plunger-diaphragm pump to the top of the reactor where it is mixed with the gaseous feed consisting of hydrogen and nitrogen, used for diluting the reactant mixture and ensuring gas phase operation. The reactor is a stainless steel tube of 0.811 m length and 0.011 m internal diameter which exhibits plug flow behaviour. The catalyst bed is placed between two layers of inert $\alpha-Al_2O_3$ particles, the bottom one serving as a physical support and the top one enhancing evaporation and ensuring preheating of the mixture up to reaction temperature. The catalyst bed itself comprises catalyst pellets and inert particles with internal diameter of 1 mm, with the mass of both ranging from 0.5 to 1 g. Dilution of the catalyst bed with dilution degree of 0.6 kg$_{dil}$kg$_{cat+dil}$$^{-1}$ ensures its axial isothermicity. The temperature inside the reactor tube can be measured and controlled by a three-point axial thermocouple placed either inside the reactor or at its outer wall. The operating pressure is maintained by means of backpressure regulator. When placed into the reactor, the catalyst is dried and further reduced at 673 K with 20% H$_2$ in N$_2$ mixture [33].

The reactor operating conditions were carefully selected within the intrinsic kinetics regime to ensure that the acquired data would be free from mass and heat transfer effects [36]. The value for the Carberry number used for assessment of mass transfer between catalyst surface and gas phase amounted to 2 10^{-5} which is 3 orders of magnitude lower than its allowed maximum. The intraparticle limitations were evaluated by Weisz-Prater criterion and considered to be negligible due to the calculated Weisz modulus of 0.00084 being sufficiently below the limit value 0.008. Heat transfer effect on the interphase and interparticle levels were assessed by calculating the corresponding temperature gradients as reported by Mears [37]. Calculated at 548 K the values for temperature gradients within the catalyst pellet and between the pellet and the bulk phase correspond to 0.007 and 0.009 K which do not exceed 2 K being the maximum allowed deviation.

The operating conditions and outlet setup section specifications, i.e. outlet lines insulation and pressure release after the reactor section, also ensured that reactor effluent remains in the gas phase until it reaches the analytical section.

For the analysis of the reactor effluent stream, the Agilent Technologies 6850 series II network GC (DB1 column) equipped with a Flame Ionization Detector (FID) was used. The calibration factors were either based on the work of Dietz [38] or determined experimentally employing calibration mixtures. The carbon balance for all the experiments was closed within 5%. This range of error allows applying the normalization method and recalculating the molar outlet flow rates assuming the closed mass balance.

The propionic acid conversion is calculated from its inlet $F_{PA,0}$ and outlet F_{PA} molar flow rates as follows:

$$X_A = \frac{F_{PA,0}-F_{PA}}{F_{PA,0}} \tag{1}$$

Every product selectivity is defined on the elemental basis using reactant and product inlet and outlet flow rates:

$$S_i = \frac{a_i(F_i-F_{i,0})}{3(F_{PA,0}-F_{PA})} \tag{2}$$

where a_i is the product i carbon number, $F_{i,0}$ and F_i are the molar

inlet and outlet flow rates of the product i. The value of 3 represents the reactant's carbon number.

A wide range of operating conditions was investigated and the experimental data were acquired after the steady state had been established. This was ensured by performing 3 consecutive analyses with 5% maximum deviation. Several operating conditions were applied per catalyst loading. A reference experiment was performed at regular time intervals to assess the long term catalyst stability and ensure constant catalyst activity. Typically, the catalyst maintained its activity during up to 30 h on stream, corresponding with 6–7 experiments per catalyst loading.

2.3. Reactor model

Considering isothermal operation and negligible pressure drop over the reactor, the 1-D pseudo-homogeneous model for plug flow can be employed, see Eq. (3):

$$\frac{dF_i}{dW} = R_i \; i = 1 ... n_{resp} \tag{3}$$

with

$$F_i = F_{i,0} \; at \; W = 0 \tag{4}$$

as initial conditions. In the above equations, W represents the catalyst mass, F_i and $F_{i,0}$ the molar outlet and inlet flowrate of the i component respectively, R_i the net production rate of component, n_{resp} number of responses.

The net formation rate R for every response is defined as the sum of rates of the reactions it is involved into taking into account the formation or consumption coefficient:

$$R_i = \sum_i \nu_{ij} r_j \tag{5}$$

where ν_{ij} is a stoichiometric coefficient of component i in reaction j. This coefficient is positive in case the component i is formed, and negative when it is consumed in the reaction. The reaction rates follow the law of mass action and are expressed as a function of the rate coefficient and the concentration of surface species and free active sites.

The flow rates of water and hydrogen were calculated based on the oxygen and hydrogen elemental balances, respectively. n-Hexane, n-octane and nitrogen, even though considered in the partial pressure calculations, were not explicitly accounted for in the final set of equations since, being inert materials, their net production rate equals zero. Eq. (3) was applied to all the responses and formed the set of differential-algebraic equations which was integrated with DDASPK, i.e., an open source code solving systems of differential-algebraic equations, available at the NETLIB software library [39].

2.4. Parameter estimation

The estimation of the kinetic parameters was performed by minimization of the weighted sum of squares of the residuals SS_{RES} between the experimental molar outlet flow rates $F_{i,j}$ and the model calculated ones $\hat{F}_{i,j}$. Adjusting the model parameter vector b was performed in a way that it approaches the real parameter β at the minimum of the objective function expressed by Eq. (6):

$$SS_{RES} = \sum_{i=1}^{n_{resp}} \sum_{j=1}^{n_{exp}} w_i (F_{i,j} - \hat{F}_{i,j})^2 (\overset{b}{\rightarrow}) min \tag{6}$$

When calculating the objective function in Eq. (6), the summation is performed over all 37 experiments ($n_{exp} = 37$), each including six responses ($n_{resp} = 6$), i.e., the molar outlet flow rates of propionic acid, ethane, methane, propane, propanol and propyl propionate.

The weighting factor w_i is calculated for each response and corresponds to the diagonal elements of the inverse of the variance-covariance matrix of the experimental error:

$$w_i = \frac{1}{\sigma_{ii}^2} = \frac{n_{exp} n_{resp} - p}{\sum_{j=1}^{n_{exp}} (F_{i,j} - \hat{F}_{i,j})^2} \tag{7}$$

where σ_{ii}^2 is the ith diagonal element of covariance matrix and p is the number of parameters.

To find the global minimum of the objective function, a combination of the Rosenbrock [40] and a Levenberg-Marquardt algorithm [41] was employed. The Rosenbrock method ensured a preliminary fast and robust approximation of the region in which the true parameter values are expected to be situated, from where the more advanced Levenberg-Marquardt algorithm can take over for the final optimization. Due to the iterative nature of the optimization algorithms, it is essential to provide initial parameter values that are as close as possible to the true ones, allowing to avoid ending up in a local minimum. The search for the best initial parameter values is typically based on previously conducted investigations as reported in the literature or retrieved from theoretical calculations [42].

In addition to the assessment of the physical meaning of the model as a whole and the individual parameters, also a statistical analysis was performed. The global significance of the model and the significance of every individual parameter was assessed by performing F and t tests, respectively. Parity diagrams were employed for visualizing the model performance. The detailed procedure for the mentioned statistical tests is reported elsewhere [43,44].

3. Results and discussion

During hydrotreatment, carboxylic acids are typically converted via two major pathways, i.e., (i) – decarbon(x)ylation with formation of light gasses (CO or CO_2) and alkanes and (ii) stepwise hydro(deoxy) genation to corresponding aldehydes, alcohols, alkenes and ultimately alkanes, i.e., fully hydrogenated products. In case acid sites are present, the produced alcohols can undergo esterification with carboxylic acids. Additionally, carboxylic acids tend to form ketones [45]. Depending on the employed catalyst and operating conditions, the generic reaction network shown in Fig. 1 can be more or less extensive.

3.1. Assessment of the operating conditions effect on the propionic acid HDO product distribution

The experimental dataset on propionic acid HDO was collected with the focus on variation of operating conditions and includes 37 experiments covering the propionic acid conversion range leading to intrinsic kinetic data acquisition. The operating conditions for these experiments range from 498 to 548 K, from 0.5 to 1.5 MPa and from 0 to 100 for the inlet molar H_2 to propionic acid ratio at space times varying between 20 and 150 kg_{cat} s mol_{PA}^{-1}. The observed product spectrum of propionic acid HDO over Ni-Cu/SiO_2-ZrO_2 catalyst comprised ethane, methane, propanol, propane, propyl propionate and trace amounts of carbon mono- and dioxide, propionaldehyde and diethyl ketone.

As expected, propionic acid conversion increases with space time, see Fig. 2a), temperature, see Fig. 4a), as well as with hydrogen partial pressure, see Fig. 5a), and total pressure, see Fig. 6a). The impact of the aforementioned operating conditions on the product distribution varies significantly. Within the entire range of the investigated operating conditions, the selectivities range between 27 and 66% for ethane, 13 and 33% for methane, 5 and 42% for propanol, 2 to 5% for propane and 3 and 14% for propyl propionate. Due to their negligible amounts in the reactor effluent, propionaldehyde and diethyl ketone were excluded from the consideration when calculating the outlet composition.

3.1.1. Conversion

As shown in Fig. 2b), increasing the space time from 20 to 117 kg_{cat} s mol_{PA}^{-1} results in a drastic decrease in the selectivity to propanol accompanied by an increase in ethane and methane selectivities, while the propionic acid conversion increases from 20 to 66%. Such a
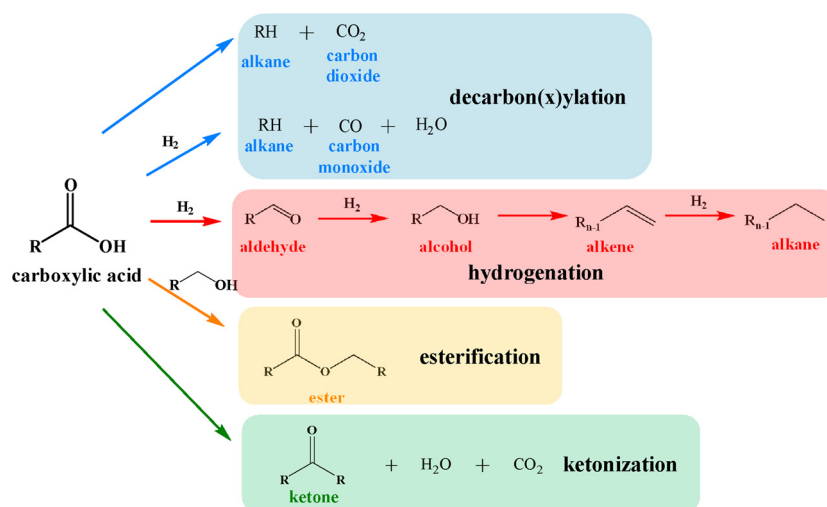
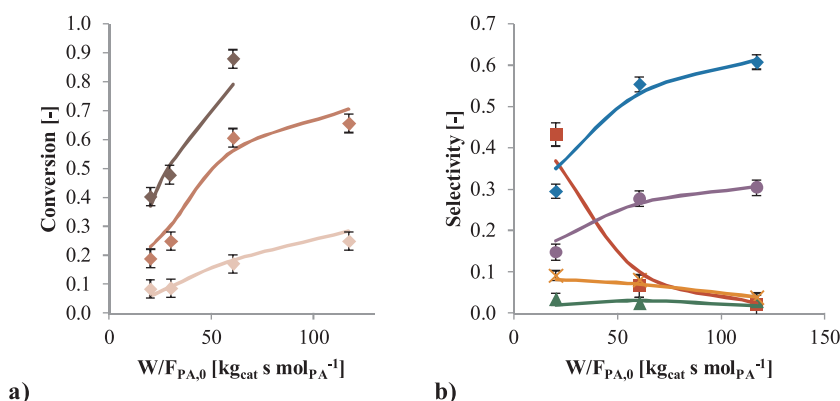**Fig. 1.** Carboxylic acid catalytic hydrotreatment reaction network.

a)

b)

Fig. 2. a) Propionic acid conversion : ◆ 498 K, ◆ 523 K, ◆ 548 K, 0,5 MPa, 38 mol_{H2} mol_{PA}^{-1} and b) product selectivities : ◆ ethane, ● methane, ■ propanol, ▲ propane, ✕ propyl propionate, 523 K, 0,5 MPa, 38 mol_{H2} mol_{PA}^{-1}, as a function of the space time on Ni-Cu/SiO$_2$-ZrO$_2$. Symbols represent experimental observations, full lines were calculated using reactor model Eq. (3) in combination with reaction rates Eq. (14)–(21) and Eq. (22). The rate and equilibrium coefficients are calculated with Eq. (23) and Eq. (24) respectively using kinetic param eter estimates listed in Table 2.
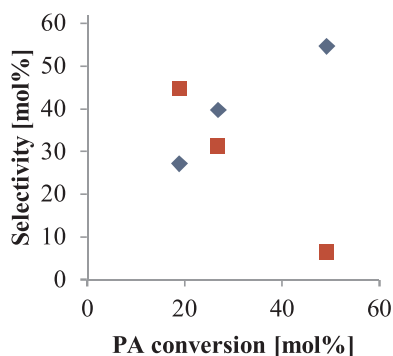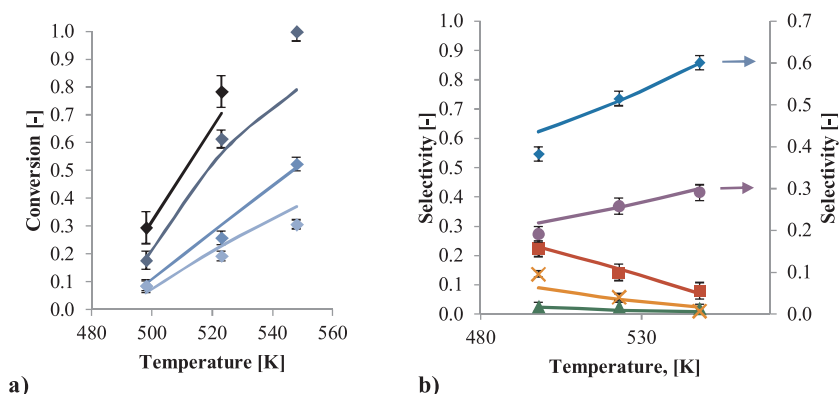

Fig. 3. First-order delplot analysis for propanol (■) and ethane (◆).

conversion induced variation in product distribution indicates the primary nature of propanol formation and the secondary, or higher order, nature of the ethane formation. Further confirmation was pursued via a so-called delplot analysis in which the selectivity is plotted versus the conversion and extrapolation to zero conversion provides information on the primary, secondary or thertary products [46]. As can be seen from the first order delplot graph shown in Figs. 3 and 4, propanol is a primary product while ethane exhibits the behavior characteristic for a secondary product. The selectivity towards propyl propionate, i.e., the esterification product between propionic acid and propanol and, hence, for sure a higher order product, decreases over the entire range of investigated operating conditions, due to the continuous decrease in propionic acid availability as well as the rapid consumption of propanol. A rather low selectivity was observed for propane in the whole

a)

b)

Fig. 4. a) Propionic acid conversion : ◆ 20 kg_{cat} s mol_{PA}^{-1}, ◆ 30 kg_{cat} s mol_{PA}^{-1}, ◆ 61 kg_{cat} s mol_{PA}^{-1}, ◆ 117 kg_{cat} s mol_{PA}^{-1}, 0.5 MPa, 38 mol_{H2} mol_{PA}^{-1} and b) product selectivities: ◆ ethane, ● - methane, ■ propanol, ▲ propane, ✕ propyl propionate, W/F$_{PA}$° varied between 20 and 117 kg_{cat} s mol_{PA}^{-1} to achieve propionic acid conversion of 30%, 0,5 MPa, 38 mol_{H2} mol_{PA}^{-1}, as a function of the temperature on Ni-Cu/SiO$_2$-ZrO$_2$. Symbols represent experimental observations, full lines were calculated using reactor model Eq. (3) in combination with reaction rates Eqs. (14)–(21) and Eq. (22). The rate and equilibrium coefficients are calculated with Eq. (23) and Eq. (24) respectively using kinetic parameter estimates listed in Table 2.
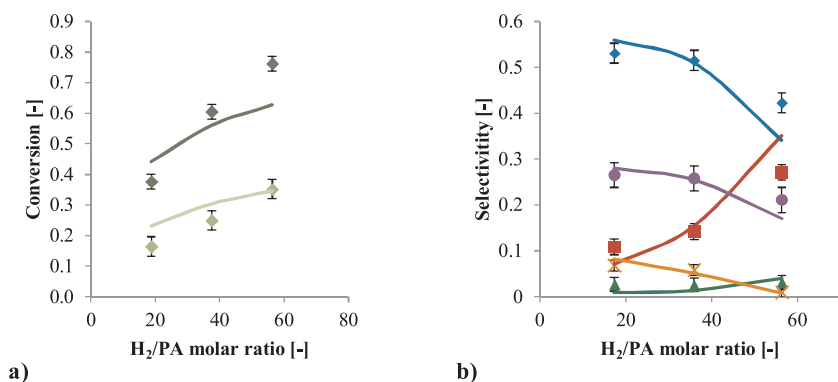
Fig. 5. a) Propionic acid conversion : $\diamond$ 30 kg_{cat} s mol_{PA}^{-1}, $\blacklozenge$ 60 kg_{cat} s mol_{PA}^{-1}, 523 K, 0.5 MPa and b) product selectivities : $\blacklozenge$ ethane, $\bullet$ methane, $\blacksquare$ propanol, $\blacktriangle$ propane, $\times$ propyl propionate, 523 K, $W/F_{PA}°$ varied between 20 and 40 kg_{cat} s mol_{PA}^{-1} to achieve propionic acid conversion of ~35%, 0,5 MPa, as a function of the hydrogen to propionic acid molar ratio on Ni-Cu/SiO$_2$-ZrO$_2$. Symbols represent experimental observations, full lines were calculated using reactor model Eq. (3) in combination with reaction rates Eqs. (14)–(21) and Eq. (22). The rate and equilibrium coefficients are calculated with Eq. (23) and Eq. (24) respectively using kinetic parameter estimates listed in Table 2.

range of investigated operating conditions. Firstly, this can be ascribed to the non-primary nature of it as a propionic acid HDO product. Secondly, the fact that even at elevated propionic acid conversion, i.e., exceeding 80%, the propane selectivity does not exceed 3%, indicates propane's slow formation compared to those of other reaction products.

To distinguish between decarbonylation and decarboxylation reactions, an experiment was performed in the absence of hydrogen, both at mild and more severe operating conditions. It led to a near to zero conversion (less than 2%) and only traces of ethane. This indicates that on the present catalyst, in the investigated range of operating conditions, ethane formation essentially requires the presence of hydrogen and, hence, occurs via the decarbonylation route, whereas decarboxylation over Ni-Cu/SiO$_2$-ZrO$_2$ catalyst is very limited and probably requires higher temperatures [47]. This is in line with previous findings over several Pd- and Ru-based catalysts [48–50].

3.1.2. Temperature

To thoroughly assess the catalyst performance, the product selectivities at different temperatures but at similar conversion were measured and compared, see Fig. 4b). A higher selectivity towards the decarbonylation products is observed at 548 K compared to that at 498 K. This is accompanied by a corresponding decrease in propanol and propyl propionate selectivities. Such a temperature effect on the product distribution is in line with previous findings in literature for aqueous-phase hydrodeoxygenation of propionic acid over Ru-based catalysts [51,52], where higher temperatures were found to facilitate C−C bond cleavage while the formation of propanol via C=O hydrogenation is preferred at lower temperatures. The observed trends, hence, indicate that the apparent activation energy for decarbonylation exceeds those for hydrogenation and esterification.

3.1.3. Inlet molar H$_2$ to propionic acid ratio

As shown in Fig. 5a), the increase in the inlet molar H$_2$ to propionic acid ratio leads to an increase in the propionic acid conversion which could be attributed to the increased hydrogenation and decarbonylation

rates, i.e., reactions that both require hydrogen as reactant. It can be assumed that this effect on the conversion will be less pronounced at higher molar ratios, where hydrogen adsorption on the catalyst surface will prevail over that of the propionic acid.

The effect on the selectivity, on the other hand, is more pronounced at higher inlet molar hydrogen to propionic acid ratio. Increasing this ratio from 17 to 36 induces only a slight increase in the selectivity to propanol from 10 to 13%, see Fig. 5b). However, a further increase of this ratio up to 56 boosts the propanol selectivity up to 41% while decreasing the ethane and methane selectivities. The observed trend can be explained by the stoichiometry of the competitive propionic acid conversion pathways. While decarboxylation does not require any hydrogen, propionic acid decarbonylation necessitates one hydrogen molecule. For propionic acid hydrogenation to propanol two hydrogen molecules are required. In that way, the initial increase in hydrogen partial pressure will enhance the rates of both decarbonylation and hydrogenation without causing dramatic difference in product selectivities. However, the further increase in hydrogen partial pressure causes the faster increase in propanol formation due to the double amount of hydrogen required in this reaction route. Despite the fact that propane is not formed to the major extent, a slight increase in its selectivity with the hydrogen partial pressure increase can be discerned and is attributed to the involvement of 3 hydrogen molecules in the full propionic acid hydrogenation to propane. The decrease in propyl propionate selectivity with the inlet molar hydrogen to propionic acid ratio can be ascribed to the absence of any explicit dependence of the esterification reaction rate on the hydrogen partial pressure and, hence, the enhancement of other reactions, rather than this esterification.

3.1.4. Total pressure

Keeping the temperature constant at 523 K, the total pressure was varied from 0.5 to 1.5 MPa, leading to an increase in propionic acid conversion from 26 to 49%, see Fig. 6a). As can be seen in Fig. 6b), experimentally, no significant pressure effect on the product distribution is observed within the range between 0.5 and 1 MPa. However,
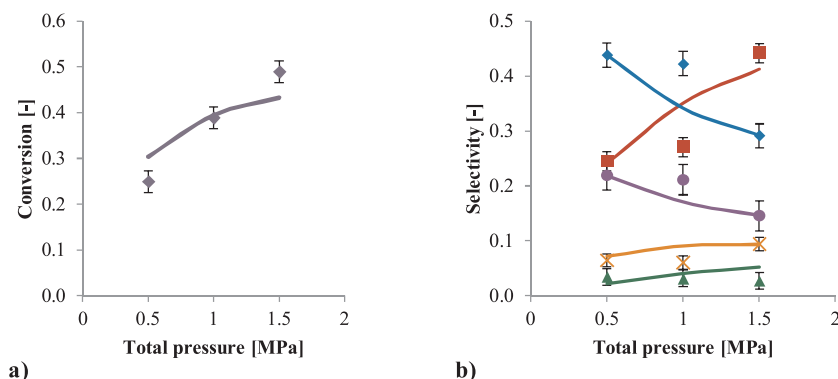

Fig. 6. a) Propionic acid conversion : $\diamond$ 30 kg_{cat} s mol_{PA}^{-1}, 523 K, 38 mol_{H2} mol_{PA}^{-1} and b) product selectivities : $\blacklozenge$ ethane, $\bullet$ methane, $\blacksquare$ propanol, $\blacktriangle$ propane, $\times$ propyl propionate, 30 kg_{cat} s mol_{PA}^{-1}, 523 K, 38 mol_{H2} mol_{PA}^{-1}, as a function of the total pressure on Ni-Cu/SiO$_2$-ZrO$_2$. Symbols represent experimental observations, full lines were calculated using reactor model Eq. (3) in combination with reaction rates Eqs. (14)–(21) and Eq. (22). The rate and equilibrium coefficients are calculated with Eq. (23) and Eq. (24) respectively using kinetic parameter estimates listed in Table 2.
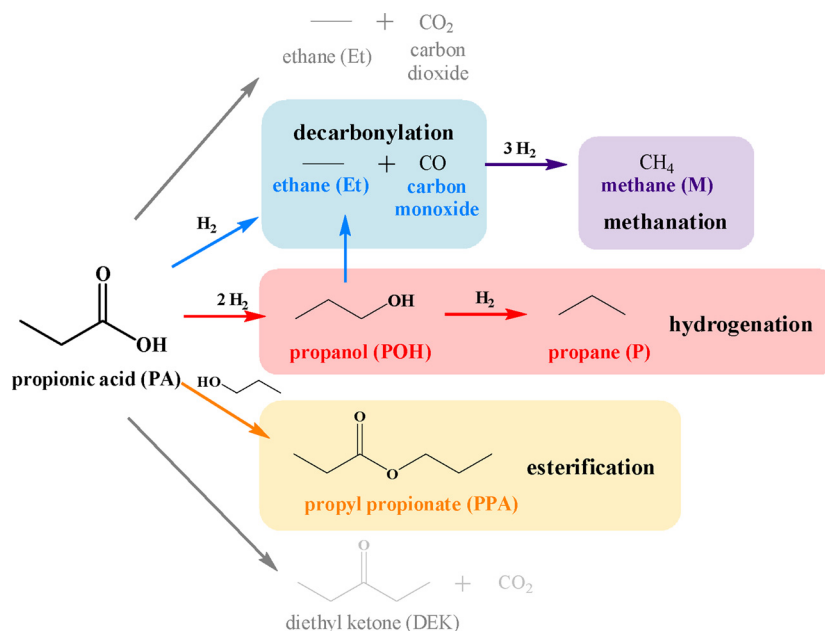
Fig. 7. Propionic acid hydrotreatment reaction network over Ni-Cu/SiO$_2$-ZrO$_2$.

further total pressure increase up to 1.5 MPa results in an increase in propanol selectivity from 27 to 44% and corresponding decrease in ethane and methane selectivities from 42 to 28% and from 20 to 14% respectively. The observed trends can be attributed to the increase of the partial pressure as well as the surface species concentration for both propionic acid and hydrogen, which follows the increase of the total pressure. As a consequence, and due to the involvement of hydrogen in the considered reactions, the increase in the hydrogenation reaction rate, where two H$_2$ molecules are required, is more pronounced than that for the decarbonylation. The increase in propyl propionate selectivity is a consequence of the increased propionic acid partial pressure as well as the trend in the propanol selectivity.

3.2. Propionic acid HDO reaction network elucidation

The above presented experimental investigation allows to identify the reactions in the general network for carboxylic acid hydrotreatment, see Fig. 1, that are relevant for propionic acid HDO over Ni-Cu/SiO$_2$-ZrO$_2$ catalyst, see Fig. 7.

One of the propionic acid conversion pathways is the hydrogenolysis of the C–O bond to propionaldehyde with water as a by-product [45,47,53]. This is followed by virtually complete hydrogenation of propionaldehyde to 1-propanol, which is one of the main reaction products [51,52]. Propane found in the reactor effluent is formed via the dehydration of propanol to propene with fast propene hydrogenation in a hydrogen-rich environment [54]. Being the final product of the hydrogenation conversion path, propane is formed in limited quantities only and, hence, not significantly affected by the variations in the operating conditions.

Propionic acid also undergoes decarbon(x)ylation to produce ethane and CO (CO$_2$). However, particularly decarboxylation was found to be very limited on the investigated catalyst within the employed operating conditions range and was not considered during kinetic modeling. Similar results were reported for fatty acids deoxygenation in the presence of Ni where CO$_2$ was formed with selectivity 10 times less than the one for CO [26]. Apart from propionic acid, within the investigated range of operating conditions, propanol was also found to undergo decarbonylation, most likely after prior dehydrogenation to propionaldehyde [55–60], which then forms ethane and CO.

Methane, which is found in the reactor effluent in equimolar quantities to ethane, is formed via methanation. Only traces of CO (and CO$_2$) were found, indicating the rapid methanation on the Ni-based catalyst in the hydrogen-rich environment. The high activity of nickel in the methanation reactions is widely reported [61,62].

Apart from the two major conversion pathways as discussed above, propionic acid is, to some extent, also converted to propyl propionate via an esterification reaction with propanol formed during hydrogenation [63]. The investigated catalyst exhibited a limited ketonization activity, which resulted in traces of 3-pentanone (diethyl ketone), i.e., below 1% selectivity. Hence, ketonization was left out of the consideration in further data analysis.

The experimental data analysis does not only allow determining the reaction network but also evaluating the catalyst performance in the investigated reaction. The Ni-Cu/SiO$_2$-ZrO$_2$ catalyst indeed ensures the occurrence of two major reactions relevant for fast pyrolysis HDO which are hydrogenation and decarbon(x)ylation. Despite the obvious benefit of decarbon(x)ylation reaction in oxygen content reduction, it is not advisable to tune a Ni based catalyst towards this reaction, given its high methanation activity, the result being an even higher hydrogen consumption than in the hydrogenation route. The hydrogenation route in propionic acid conversion over Ni-Cu/SiO$_2$-ZrO$_2$ is favored at lower temperatures, higher total pressures and inlet molar hydrogen to propionic acid ratios. However, full hydrogenation of the propionic acid to propane occurs only to a very limited extent, even at high conversion levels. Being capable to convert the reactive components of fast pyrolysis oil to more stable ones and partially remove the oxygen content already at mild operating conditions, Ni-Cu/SiO$_2$-ZrO$_2$ indeed acts as an excellent stabilization catalyst [33,64]. However, when used as a catalyst for the deep HDO stage, it tends to facilitate decarbon(x)ylation followed by methanation which leads to carbon losses and high hydrogen consumption levels. Additionally, Ni-Cu/SiO$_2$-ZrO$_2$ shows very limited selectivity to fully hydrodeoxygenated products requiring hydrogenation activity, which appears as a major drawback for the deep HDO catalyst.

3.3. Kinetic modeling

Apart from the qualitative reaction network identification and the general considerations on the catalyst performance, the acquired experimental data were also used as an input for kinetic model
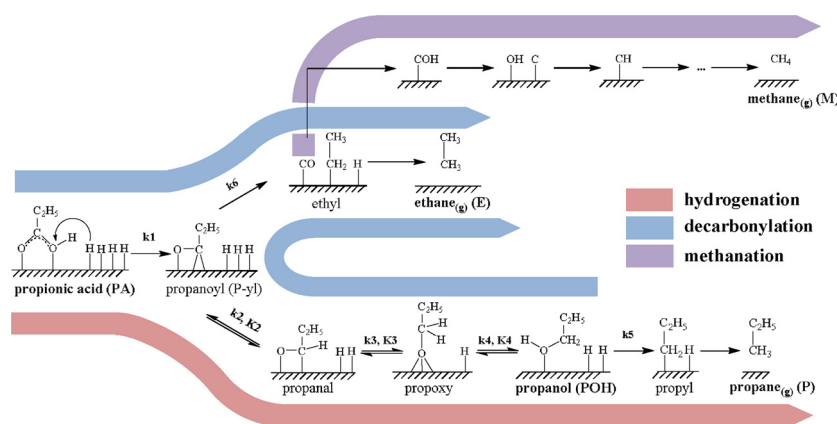
Fig. 8. Comprehensive propionic acid hydrotreatment reaction network on the metal active sites.

construction on propionic acid HDO over Ni-Cu/SiO$_2$-ZrO$_2$ catalyst.

When constructing a kinetic model it is of utmost importance to determine its level of complexity, which is highly correlated with the goal pursued. If the aim is the determination of relations between operating conditions and reactor outlet composition under a specific narrow set of operating conditions, power law models are typically sufficient. Such models are characterized by straightforward procedures for their construction and rather good fitting to experimental data, however, they only account for global reactions and do not provide specific information on the elementary steps on the catalyst surface. When a more detailed understanding of the catalytic reaction mechanism is pursued, the corresponding kinetic model should be based on the elementary steps including adsorption, surface reaction and desorption of the reactants and products involved. Langmuir-Hinshelwood-Hougen-Watson (LHHW) type of kinetic models account for both surface reaction mechanisms and adsorption by means of Langmuir isotherm. While being simplified by using a rate-determining step concept, LHHW models still provide sufficient information on the reaction mechanism and adsorption on the catalyst surface with a reasonable amount of effort involved [28,65].

3.3.1. Reaction mechanism

In order to construct a fundamental kinetic model for propionic acid hydrotreatment it is essential to establish the reaction mechanism in a way that each global reaction, i.e., hydrogenation, decarbonylation and esterification, is described in terms of elementary steps. Based on the experimentally observed trends, complemented with extensive literature information [48–50,52,53,56,58,59,61,62,66–69], the global scheme as reported in Fig. 7 can be transformed into the proposed mechanism for Ni-catalyzed reactions as represented in Fig. 8.

After being adsorbed on the catalyst surface, propionic acid is assumed to undergo hydrogen assisted C–OH bond cleavage with formation of a surface-bound acyl radical of propionic acid (propanoyl) and a water molecule [66,70]. Further hydrogenation of the propanoyl species results in propionaldehyde formation. Since practically no aldehyde was detected in the reactor effluent, it was considered that propionaldehyde does not desorb from the catalyst surface but rather undergoes further hydrogenation to propanol via a propoxy species [52,55,66]. The propanoyl species can alternatively dehydrate and undergo C−CO bond scission to produce carbon monoxide and ethyl

species which are further hydrogenated to ethane [48–50]. The formed propanol can be further dehydrated to propyl which is hydrogenated to propane in a hydrogen-rich environment [71,72]. Propanol decarbonylation occurs in the same sequence of the reactions as propionic acids hydrogenation but happening in the opposite direction: propoxy formed via dehydrogenation of propanol undergoes further dehydrogenation to propanal, which after loosing one more hydrogen atom forms propanoyl being the intermediate species leading to ethane and carbon monoxide [55–60].

Due to the experimental evidence, it can be concluded that all the CO formed during the decarbonylation is further methanated. Though being extensively studied, the detailed CO methanation mechanism remains a matter of debate. Two main methanation reaction pathways are typically reported in the literature, i.e., one where stepwise hydrogenation follows direct carbon monoxide dissociation on the surface into C and O species [69,73], and another one where CO dissociation occurs through the hydrogen attack on the oxygen of CO [74,75]. However, for the purpose of the kinetic modelling performed in the present work it is of less importance to chose between the debated mechanisms since methanation on the studied catalyst was considered to happen fast and irreversibly.

The esterification between carboxylic acids and alcohols is catalyzed by Bronsted or Lewis acids. Although homogeneous catalysis is more commonly employed for esterification reactions, heterogeneous catalysts, including solid metal oxides, are not uncommon [76]. In the present case, it is most likely that propionic acid esterification with propanol takes place on SiO$_2$-ZrO$_2$ which is known to be a Lewis acid, rather than on metal sites of the Ni-Cu/SiO$_2$-ZrO$_2$ catalyst. The introduction of propionic acid together with propanol to the reactor filled with pure ZrO$_2$ resulted in propyl propionate formation, verifying the proposed assumption. According to the reaction mechanism for esterification of fatty acids catalyzed by metal oxides proposed by Suarez et al. [68], the alcohol dissociatively adsorbs on the metal oxide and forms alkoxide and hydroxyl. The latter is further protonated to form water, whereas the alkoxide ligand attacks the carbonyl group of the acid and forms the final product, i.e., the ester. According to this mechanism, the metal oxide sites would be only occupied by propanol and the esterification product, i.e., propyl propionate, while propionic acid reacts with the hydroxyl directly from the gas phase forming the next reaction intermediate on the same active site, see Fig. 9.
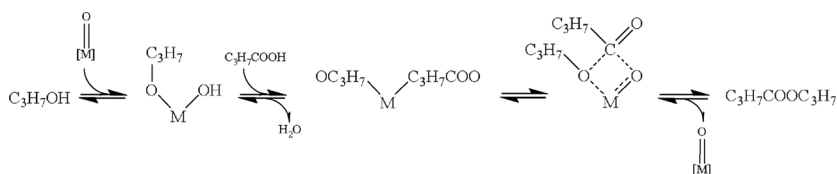
Fig. 9. Esterification reaction mechanism over SiO$_2$-ZrO$_2$ active sites (adopted from [68]).

Table 1

Propionic acid HDO elementary steps with the corresponding kinetic descriptors.

Global reaction	Elementary step	Kinetic descriptor
Reactant adsorption	$PA + * \rightleftharpoons PA^*$	K_{PA}
	$H_2 + 2* \rightleftharpoons 2H^*$	K_{H2}
Propionic acid hydrogenation to propanol	$PA^* + H^* \rightarrow P{-}yl^* + H_2O + *$	k_1
	$P{-}yl^* + H^* \rightleftharpoons P{-}al^* + *$	k_2, K_2
	$P{-}al^* + H^* \rightleftharpoons Propoxy^* + *$	k_3, K_3
	$Propoxy^* + H^* \rightleftharpoons POH^* + *$	k_4, K_4
Propanol hydrogenation to propane	$POH^* + H^* \rightarrow Propyl^* + H_2O + *$	k_5
Decarbonylation	$P{-}yl* \rightarrow Ethyl^* + CO^*$	k_6
Methanation	$P{-}yl* \rightarrow Ethyl^* + CO^*$	k_6
Esterification	$POH^\Delta + PA \rightleftharpoons PPA^\Delta + H_2O$	k_{est}, K_{est}
Product desorption	$POH^* \rightleftharpoons POH + *$	K_{POH}
	$POH^\Delta \rightleftharpoons POH + \Delta$	$K_{POH}{}'$
	$PPA^\Delta \rightleftharpoons PPA + \Delta$	K_{PPA}

3.3.2. Kinetic model development and reaction rate expressions derivation

Based on the mechanism proposed in Section 3.3.1, the kinetic model for propionic acid HDO was constructed. All the elementary steps with the corresponding kinetic parameters are summarized in Table 1.

Regarding hydrogen adsorption on the Ni surface, some studies propose competitive adsorption [77,78], while others suggest that hydrogen adsorbs on active sites distinct from those for the organic adsorbates [79,80]. It was assumed that hydrogen is adsorbed dissociatively and competes for the same active sites as propionic acid and surface reaction products. This assumption allows to significantly simplify the reaction rate expressions as well as to reduce the number of parameters to be estimated. Moreover, as it has been discussed previously, the modeling efforts as required for a dual site mechanism do not always outweigh the benefits of an improved model performance compared to the experimental observations [77,81,82]. Since it is widely reported that alkanes rather weakly adsorb on the metal surfaces [49], it was decided to consider methane, ethane and propane desorption from the Ni surface as fast and irreversible. The adsorption of water was also neglected [70]. The adsorption of the remaining products as well as the reactants was assumed to be quasi-equilibrated, which results in the following expressions for the surface concentrations of the adsorbed species:

$$[i^*] = [*]K_i p_i \tag{8}$$

$$[H^*] = [*]\sqrt{K_{H_2}p_{H_2}} \tag{9}$$

As discussed in Section 3.3.1, the proposed mechanism suggests that hydrogenation, decarbonylation and methanation take place on Ni metal active sites and esterification on the acidic metal oxide sites, i.e., SiO$_2$-ZrO$_2$. In this case, two site balances are required. Assuming that hydrogen adsorbs dissociatively on Ni and that propanol can be adsorbed on both Ni and SiO$_2$-ZrO$_2$, the site balance for Ni and SiO$_2$-ZrO$_2$ is expressed by Eqs. (10) and (11) respectively. The concentration of the intermediate species was considered low compared to those of reactants and, thus, was not accounted for in the presented expressions for active site balances.

$$[*]_{tot} = [*] + [PA^*] + [H^*] + [POH^*] \tag{10}$$

$$[\Delta]_{tot} = [\Delta] + [POH^\Delta] + [PPA^\Delta] \tag{11}$$

where * represents the metal active site and Δ the metal oxide site.

The proposed mechanism involves 19 elementary steps taking place on the catalyst surface: 17 reactions on Ni and 2 on SiO$_2$-ZrO$_2$. The reaction rate of the surface elementary steps can be expressed using the law of mass action:

$$r_j = k_j \prod [i^*]^{\nu_{ij}} \tag{12}$$

For the reverse reactions the reaction rate coefficient was expressed via the forward reaction rate coefficient and reaction equilibrium coefficient:

$$k_{-j} = \frac{k_j}{K_j} \tag{13}$$

The pseudo-steady state approximation was applied to the concentration of the intermediate species, i.e., their net production rate was set equal to zero. The resulting set of equations comprises six ordinary differential equations for propionic acid, propanol, propane, ethane, methane and propyl propionate (Eq.(14), Eqs. (18)–(21)), and three algebraic equations determining the concentration of the intermediate species, i.e., propanoyl, propionaldehyde and propoxy (Eqs. (15)–(17)).

$$\frac{dF_{PA}}{dW} = -k_1[PA^*][H^*] - k_{est}[POH^\Delta]p_{PA} + \frac{k_{est}}{K_{est}}[PPA^\Delta][\Delta] \tag{14}$$

$$k_1[PA^*][H^*] - k_2[Propanoyl^*][H^*] + \frac{k_2}{K_2}[Propanal^*][*] - k_5\left[POH\right][H^*] = 0 \tag{15}$$

$$k_2[Propanoyl^*][H^*] - \frac{k_2}{K_2}[Propanal^*][*] - k_3[Propanal^*][H^*] + \frac{k_3}{K_3}[Propoxy^*][*] = 0 \tag{16}$$

$$k_3[Propanal^*][H^*] - \frac{k_3}{K_3}[Propoxy^*][*] - k_4[Propoxy^*][H^*] + \frac{k_4}{K_4}[POH^*][*] = 0 \tag{17}$$

$$\frac{dF_{POH}}{dW} = k_4[Propoxy^*][H^*] - \frac{k_4}{K_4}[POH^*][*] - k_5\left[POH\right][H^*] - k_{est}[POH^\Delta]p_{PA} + \frac{k_{est}}{K_{est}}[PPA^\Delta][\Delta] \tag{18}$$

$$\frac{dF_P}{dW} = k_5[POH^*][H^*] - k_{est}[POH^\Delta]p_{PA} + \frac{k_{est}}{K_{est}}[PPA^\Delta][\Delta] \tag{19}$$

$$\frac{dF_E}{dW} = \frac{dF_M}{dW} = k_7[Propanoyl^*][*] \tag{20}$$

$$\frac{dF_{PPA}}{dW} = k_{est}[POH^\Delta]p_{PA} - \frac{k_{est}}{K_{est}}[PPA^\Delta][\Delta] \tag{21}$$

Application of the Langmuir assumptions with respect to adsorption results in the following expression for the surface concentrations of reactants and products:

$$[i^*] = \frac{[*]_{tot} K_i p_i}{1 + \sum K_i p_i} \tag{22}$$

Combination of Eqs. (14)–(21) with Eq.(22) leads to the final set of DAE which is further integrated using the DDASPK solver.

3.3.3. Parameters definition and model assessment

The constructed kinetic model features a total of 16 coefficients, amongst which 7 rate coefficients, 4 surface reaction equilibrium coefficients and 5 adsorption coefficients. The temperature dependence of the rate and equilibrium coefficients is expressed by the Arrhenius equation, see Eq. (23), and Van't Hoff equation, see Eq. (24), respectively:

$$k_j = A_j e^{-E_{a,j}/RT} \tag{23}$$

$$K_i = e^{\Delta S_i^0/R} e^{-\Delta H_i^0/RT} \tag{24}$$

where A_j is the pre-exponential factor, $E_{a,j}$ is the activation energy, ΔS_i^0 is the standard reaction or adsorption entropy and ΔH_i^0 is the standard reaction or adsorption enthalpy. It doubles the number of model parameters to be determined to 32. In order to reduce this number of parameters to be estimated by regression, values for pre-exponential factors and equilibrium entropies for surface reaction and adsorption were calculated a-priori based on statistical thermodynamics and kept fixed during further regression [42].

Employing transition state theory, the pre-exponential factor can be expressed according to Eq. (25):

$$A_j = \frac{k_B T}{h} e^{\Delta S_j^{\neq}/R} \tag{25}$$

where k_B is the Boltzmann constant, h the Plank constant and $\Delta S_j^{\neq}$ the entropy difference between the reactant and transition state. The $\Delta S_j^{\neq}$ term stems from changes in species mobility due to the transformation from the initial to the transition state. It is typically calculated based on well-considered assumptions on the loss of or gain in degrees of freedom during the latter change. The entropy change due to

adsorption is generally quantified as a loss of translational degrees of freedom, as approximated by the Sackur-Tetrode equation [83]. In line with literature, the loss of two degrees of freedom was considered during the adsorption of propionic acid and propanol [44,84]. Due to the dissociative character of hydrogen adsorption together with the assumption of hydrogen adsorption on the metal surface being weaker than that of propionic acid, the loss of only one degree of freedom was accounted for in case of hydrogen. The obtained values for the pre-exponential factors as well as the adsorption and reaction entropies are listed in Table 2. The total concentration of metal active sites was determined by CO chemisorption and corresponds to $378\,\text{mmol kg}_{\text{cat}}^{-1}$ [33]. Since no direct measurements of the acidity was performed for the studied catalyst, the concentration of the metal oxide active sites was fixed at $100\,\text{mmol kg}_{\text{cat}}^{-1}$ which corresponds to the values obtained for the similar Ni-Cu/SiO$_2$-ZrO$_2$ catalyst via NH$_3$-TPD by Heeres et al. [85].

Ultimately, the proposed kinetic model for propionic acid HDO over Ni-Cu/SiO$_2$-ZrO$_2$ catalyst contains 16 adjustable parameters, in particular 7 activation energies, $E_{a,j}$, 4 surface reaction enthalpies, ΔH_j, and 5 adsorption enthalpies, ΔH_i^0.

3.3.4. Regression analysis and model performance evaluation

Non-isothermal, weighted regression of the proposed kinetic model to the intrinsic kinetic data acquired for propionic acid HDO over Ni-Cu/SiO$_2$-ZrO$_2$ catalyst resulted in estimates for activation energies, surface reaction and adsorption enthalpies as presented in Table 2. The F value for the global significance of the regression amounted to 700 which exceeds the tabulated value of 2.79. All 16 model parameters were estimated statistically significant and with very narrow confidence intervals.

The estimated activation energies increase in the following order:

$$E_{a,2} < E_{a,4} < E_{a,5} < E_{a,est} < E_{a,3} < E_{a,7} < E_{a,1} \tag{26}$$

The lowest activation energies were obtained for propanoyl and propoxy hydrogenation to propionaldehyde and propanol respectively, their values amounting to 14.8 and $27.1\,\text{kJ mol}^{-1}$. When compared to the activation energy of propionaldehyde hydrogenation, which amounts to $83.9\,\text{kJ mol}^{-1}$, these values indicate the potential quasi-equilibrated nature of the related elementary steps, as confirmed by the values of the corresponding rate coefficients at 523 K. That would propose that the formation of propanol from the propanoyl species on the catalyst surface is mainly determined by the reaction rate of the propionaldehyde hydrogenation. Propanoyl and propoxy hydrogenation proceed at much higher rates and the propanoyl and propoxy concentration on the catalyst surface are rather determined by the surface reaction equilibrium coefficients K_2 and K_4.

The relatively low activation energy for propane formation, $E_{a,5} = 30.5\,\text{kJ mol}^{-1}$, and the correspondingly high value for the rate coefficient indicate that propanol hydrodeoxygenation reaction is potentially fast on the investigated catalyst surface. However, the analysis of experimental data showed a very low propane concentration in the reactor effluent. This low selectivity towards propane (2–5 %) can be ascribed to the low value calculated by the model for the propanol adsorption equilibrium coefficient on the Ni surface ($K_{POH}^{523} = 6.8\ 10^{-5}$), i.e., propanol after being formed is more likely to desorb from the catalyst surface than undergo further hydrodeoxygenation.

It was evident from the model parameter estimates that propanol, although formed on Ni, has a higher affinity to metal oxide active sites as indicated by the high propanol adsorption enthalpy ($104.2\,\text{kJ mol}^{-1}$) on SiO$_2$-ZrO$_2$ and the 8 orders of magnitude higher value for the respective adsorption coefficient than the one calculated for nickel active sites. The ratio between adsorption enthalpies $-\Delta H_{POH}^0$ and $-\Delta H_{POH}^0{}'$ explains the higher selectivity to propyl propionate then the one to propane despite of the higher activation energy of propyl propionate formation. Simultaneously, the more pronounced temperature dependence of the propyl propionate selectivity compared to that of propane, see Fig. 4b), can be attributed to the higher activation energy by
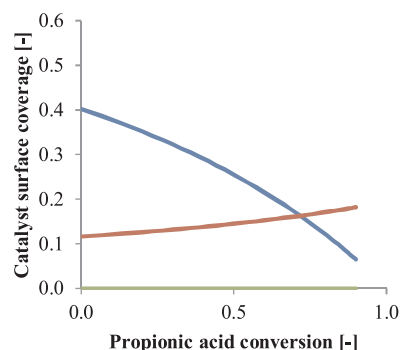
Table 2

Model kinetic parameter values including a-priori calculated values for reaction pre-exponential factors, reaction and adsorption entropies and parameter estimates for the reaction activation energies, reaction and adsorption enthalpies along with the corresponding 95% individual confidence interval obtained from the weighted non-isothermal regression following the proposed mechanism.

	$\Delta S_i^0\ [J\ mol^{-1}\ s^{-1}]$	$-\Delta H_i^0\ [kJ\ mol^{-1}]$	K_i^{523}
K_{PA}	−139	93.8 ± 0.6	1.3 10^2
K_{H2}	−64	27.3 ± 1.2	2.4 10^{-1}
K_{POH}	−138	30.5 ± 1.3	6.8 10^{-5}
$K_{POH}{}'$	−138	104.2 ± 1.8	1.6 10^3
K_{PPA}	−106	44.8 ± 2.8	8.7 10^{-2}

	$A_j\ [kg_{cat}\ mol^{-1} s^{-1}]$	$E_{a,j}\ [kJ\ mol^{-1}]$	k_j^{523}
k_1	10^{12}	118.4 ± 0.5	3.8 10^{-1}
k_2	10^9	14.8 ± 0.8	9.3 10^7
k_3	10^{10}	83.9 ± 2.1	9 10^1
k_4	10^9	27.1 ± 1.2	7.7 10^6
k_5	10^9	30.5 ± 1.5	7.1 10^5
k_6	10^{10}	97.6 ± 1.7	2.9
k_{est}	10^{11}	55.7 ± 0.8	6.8 10^5

	$\Delta S_j^0\ [J\ mol^{-1}\ s^{-1}]$	$-\Delta H_j^0\ [kJ\ mol^{-1}]$	K_j^{523}
K_2	−0.1	0.8 ± 0.03	1.2
K_3	−48.6	5.0 ± 0.35	9 10^{-3}
K_4	−43.4	3.2 ± 0.14	1 10^{-2}
K_{est}	9.1	0.7 ± 0.05	3.5

Fig. 10. Calculated Ni surface coverage plotted against propionic acid conversion, (— θ_{PA}, — θ_{H2}, — θ_{POH}), 523 K, 0.5 MPa, 38 $mol_{H2}\ mol_{PA}^{-1}$. The simulation was performed using reactor model Eq. (3) in combination with reaction rates Eqs. (14)–(21) and Eq. (22). The rate and equilibrium coefficients are calculated with Eq. (23) and Eq. (24) respectively using kinetic parameter estimates listed in Table 2.
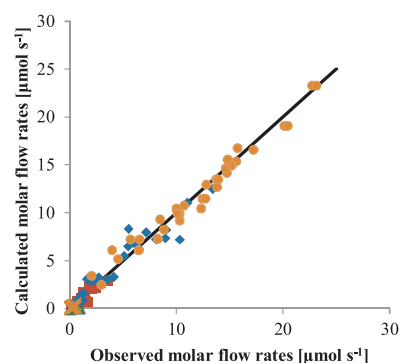

Fig. 11. Parity diagram for the outlet molar flow rates of the propionic acid hydrotreatment (◆ ethane, ● propionic acid, ■ propanol, ▲ propane, × propyl propionate).

25 kJ mol^{-1} for the esterification reaction.

The highest activation energy in the kinetic model was obtained for the first step preceding both hydrogenation and decarbonylation pathways. The high value for the C–OH bond cleavage activation energy is in agreement with DFT values computed for acetic acid on noble metal surfaces [66]. Moreover, propanoyl formation from propionic acid has been identified as the rate-determining step on Ni as well as on Pd surfaces [66].

The experimentally observed increase in ethane selectivity with the temperature, see Fig. 4b), is captured adequately by the model and attributed to the higher activation energy of propanoyl decomposition, $E_{a,7} = 97.6$ kJ mol^{-1}, compared to those of other product formation reactions.

Relatively low values were estimated for surface reaction equilibrium coefficients $K_2 = 1.2$, $K_3 = 0.009$, $K_4 = 0.01$, implying that surface reaction equilibria are rather favoring the reactants.

The catalyst surface was simulated not to be saturated in the investigated range of operating conditions and to contain propionic acid as the most abundant surface species despite the molar excess of hydrogen, see Fig. 10. Such trend of the various species concentration on the catalyst surface explains the high selectivity to decarbonylation, a reaction requiring twice less hydrogen compared to hydrogenation, despite its relatively high activation energy and low rate coefficient. The increase in hydrogen partial pressure results in an analogous increase of hydrogen concentration on the surface which facilitates the formation of the hydrogenation products, a phenomenon captured correctly by the model, as shown in Fig. 5.

The parity diagram, see Fig. 11, as well as the performance curves, see Figs. 2–6, demonstrate the capability of the model of adequately

describing the propionic acid hydrotreatment within a wide range of operating conditions. The calculated outlet flow rates for all the components are in a very good agreement with the experimentally observed ones, especially when describing the conversion, temperature and inlet composition effect, see Figs. 2, 4 and 5 respectively. Slight deviations can be observed in the case of the total pressure effect, that could be possibly ascribed to the assumption of fast and irreversible alkanes desorption which can become less relevant with the pressure increase. Yet the model still captures the main trends in product selectivities, see Fig. 6b).

4. Conclusions

Intrinsic kinetics for the propionic acid hydrotreament were measured on a Ni-Cu/SiO$_2$-ZrO$_2$ catalyst over a wide range of operating conditions. Two major reaction pathways, i.e., decarbonylation to ethane and hydrodeoxygenation to propanol and propane were identified. Additionally, esterification between propionic acid and propanol yielded propyl propionate and was ascribed to the presence of metal oxides SiO$_2$-ZrO$_2$ in the catalyst composition. Decarboxylation and ketonization did not occur to a significant extent. The analysis of the experimental data revealed the secondary nature of ethane stemming from the decarbonylation of the propionic acid hydrogenation product – propanol.

Ni-Cu/SiO$_2$-ZrO$_2$ appeared to be a suitable catalyst for fast pyrolysis oil stabilization since at mild operating conditions, typical for stabilization rather than deep oxygen removal, it tends to favor hydrogenation rather than decarbonylation. Particularly on Ni based catalysts with a pronounced methanation activity, despite the lower hydrogen consumption during the actual decarbonylation, it is, nevertheless an undesirable one given the pronounced hydrogen consumption by methanation. Moreover, Ni-Cu/SiO$_2$-ZrO$_2$ showed limited activity towards full hydrodeoxygenation of propionic acid to propane which, again, proposes this catalyst to be more beneficial at the stabilization rather than at the deep HDO stage of fast pyrolysis oil hydrotreatment.

To quantitatively describe the observed trends, a comprehensive kinetic model for propionic acid hydrotreatment was developed. Being based on elementary adsorption, surface reaction and desorption steps, this model was capable of adequately describing the experimental data and providing more insight into the reaction mechanism. The assumption of dissociative hydrogen adsorption on the same active sites as propionic acid and reaction products did not cause any inconsistency during the modeling work and, thus, proved to be valid. The rate-limiting step was identified to be propionic acid activation, i.e., C–OH bond cleavage, which is a step preceding both hydrodeoxygenation and decarbonylation. From the 3 consecutive steps leading to propanol, propionaldehyde hydrogenation has the lowest rate coefficient with the highest activation energy, whereas propanoyl and propoxy hydrogenation tend to be quasi-equilibrated. The propane yield was found to be lower than that of propyl propionate due to the lower affinity of propanol to metal surface compared to that of metal oxides.

References

[1] IEA, Energy to 2050: Scenarios for a Sustainable Future, OECD Publishing, 2013.
[2] BP, BP Statistical Review of World Energy, 2017.
[3] C.H. Lam, S. Das, N.C. Erickson, C.D. Hyzer, M. Garedew, J.E. Anderson,

T.J. Wallington, M.A. Tamor, J.E. Jackson, C.M. Saffron, Towards sustainable hydrocarbon fuels with biomass fast pyrolysis oil and electrocatalytic upgrading, Sustain. Energy Fuels 1 (2017) 258–266.

[4] A.V. Bridgwater, Review of fast pyrolysis of biomass and product upgrading, Biomass Bioenergy 38 (2012) 68–94.

[5] J.A. Melero, J. Iglesias, A. Garcia, Biomass as renewable feedstock in standard refinery units. Feasibility, opportunities challenges, Energy Environ. Sci. 5 (2012) 7393–7420.

[6] D. Carpenter, T. Westover, D. Howe, S. Deutch, A. Starace, R. Emerson, S. Hernandez, D. Santosa, C. Lukins, I. Kutnyakov, Catalytic hydroprocessing of fast pyrolysis oils: Impact of biomass feedstock on process efficiency, Biomass Bioenergy 96 (2017) 142–151.

[7] J.C. Serrano-Ruiz, J.A. Dumesic, Catalytic routes for the conversion of biomass into liquid hydrocarbon transportation fuels, Energy Environ. Sci. 4 (2011) 83–99.

[8] B.M.Q. Phan, L.T. Duong, V.D. Nguyen, T.B. Tran, M.H.H. Nguyen, L.H. Nguyen, D.A. Nguyen, L.C. Luu, Evaluation of the production potential of bio-oil from Vietnamese biomass resources by fast pyrolysis, Biomass Bioenergy 62 (2014) 74–81.

[9] E. Furimsky, Hydroprocessing challenges in biofuels production, Catal. Today 217 (2013) 13–56.

[10] H. Kobayashi, H. Ohta, A. Fukuoka, Conversion of lignocellulose into renewable chemicals by heterogeneous catalysis, Catal. Sci. Technol. 2 (2012) 869–883.

[11] H. Wang, J. Male, Y. Wang, Recent advances in hydrotreating of pyrolysis bio-oil and its oxygen-containing model compounds, ACS Catal. 3 (2013) 1047–1070.

[12] K. Hengst, M. Schubert, W. Kleist, J.-D. Grunwaldt, Hydrodeoxygenation of Lignocellulose-Derived Platform Molecules, Catalytic Hydrogenation for Biomass Valorization, The Royal Society of Chemistry, 2015, pp. 125–150 Chapter 6.

[13] T. Prasomsri, T. Nimmanwudipong, Y. Roman-Leshkov, Effective hydrodeoxygenation of biomass-derived oxygenates into unsaturated hydrocarbons by MoO3 using low H2 pressures, Energy Environ. Sci. 6 (2013) 1732–1738.

[14] D.E. Resasco, What Should We Demand from the Catalysts Responsible for Upgrading Biomass Pyrolysis Oil? ACS Publications, 2011.

[15] R.J. French, S.K. Black, M. Myers, J. Stunkel, E. Gjersing, K. Iisa, Hydrotreating the organic fraction of biomass pyrolysis oil to a refinery intermediate, Energy Fuel 29 (2015) 7985–7992.

[16] S.R.A. Kersten, W.P.M. van Swaaij, L. Lefferts, K. Seshan, Options for Catalysis in the Thermochemical Conversion of Biomass into Fuels, Catalysis for Renewables, Wiley-VCH Verlag GmbH & Co. KGaA, 2007, pp. 119–145.

[17] R.H. Venderbosch, A.R. Ardiyanti, J. Wildschut, A. Oasmaa, H.J. Heeres, Stabilization of biomass-derived pyrolysis oils, J. Chem. Technol. Biotechnol. 85 (2010) 674–686.

[18] D. Kubička, J. Horáček, Deactivation of HDS catalysts in deoxygenation of vegetable oils, Appl. Catal. A 394 (2011) 9–17.

[19] T.R. Viljava, R.S. Komulainen, A.O.I. Krause, Effect of H2S on the stability of CoMo/Al2O3 catalysts during hydrodeoxygenation, Catal. Today 60 (2000) 83–92.

[20] V.A. Yakovlev, S.A. Khromova, O.V. Sherstyuk, V.O. Dundich, D.Y. Ermakov, V.M. Novopashina, M.Y. Lebedev, O. Bulavchenko, V.N. Parmon, Development of new catalytic systems for upgraded bio-fuels production from bio-crude-oil and biodiesel, Catal. Today 144 (2009) 362–366.

[21] E. Laurent, B. Delmon, Study of the hydrodeoxygenation of carbonyl, carboxylic and guaiacyl groups over sulfided CoMo/γ-Al2O3 and NiMo/γ-Al2O3 catalysts, Appl. Catal. A 109 (1994) 77–96.

[22] A. Gutierrez, R.K. Kaila, M.L. Honkela, R. Slioor, A.O.I. Krause, Hydrodeoxygenation of guaiacol on noble metal catalysts, Catal. Today 147 (2009) 239–246.

[23] S. De, J. Zhang, R. Luque, N. Yan, Ni-based bimetallic heterogeneous catalysts for energy and environmental applications, Energy Environ. Sci. 9 (2016) 3314–3347.

[24] Y. Wang, S. De, N. Yan, Rational control of nano-scale metal-catalysts for biomass conversion, Chem. Commun. 52 (2016) 6210–6224.

[25] E. Santillan-Jimenez, T. Morgan, J. Lacny, S. Mohapatra, M. Crocker, Catalytic deoxygenation of triglycerides and fatty acids to hydrocarbons over carbon-supported nickel, Fuel 103 (2013) 1010–1017.

[26] W. Li, Y. Gao, S. Yao, D. Ma, N. Yan, Effective deoxygenation of fatty acids over ni (OAc)2 in the absence of H2 and solvent, Green Chem. 17 (2015) 4198–4205.

[27] A.G. Hansen, W.J.M. van Well, P. Stoltze, Microkinetic modeling as a tool in catalyst discovery, Top. Catal. 45 (2007) 219–222.

[28] J.W. Thybaut, G.B. Marin, Single-event microkinetics: catalyst design for complex reaction networks, J. Catal. 308 (2013) 352–362.

[29] M.V. Bykova, O.A. Bulavchenko, D.Y. Ermakov, M.Y. Lebedev, V.A. Yakovlev, V.N. Parmon, Guaiacol hydrodeoxygenation in the presence of ni-containing catalysts, Catal. Ind. 3 (2011) 15–22.

[30] M.V. Bykova, D.Y. Ermakov, V.V. Kaichev, O.A. Bulavchenko, A.A. Saraev, M.Y. Lebedev, V.A. Yakovlev, Ni-based sol–gel catalysts as promising systems for crude bio-oil upgrading: Guaiacol hydrodeoxygenation study, Appl. Catal. B: Environ. 113–114 (2012) 296–307.

[31] M.V. Bykova, D.Y. Ermakov, S.A. Khromova, A.A. Smirnov, M.Y. Lebedev, V.A. Yakovlev, Stabilized Ni-based catalysts for bio-oil hydrotreatment: reactivity studies using guaiacol, Catal. Today 220–222 (2014) 21–31.

[32] A.R. Ardiyanti, M.V. Bykova, S.A. Khromova, W. Yin, R.H. Venderbosch, V.A. Yakovlev, H.J. Heeres, Ni-based catalysts for the hydrotreatment of fast pyrolysis oil, Energy Fuel 30 (2016) 1544–1554.

[33] W. Yin, A. Kloekhorst, R.H. Venderbosch, M.V. Bykova, S.A. Khromova, V.A. Yakovlev, H.J. Heeres, Catalytic hydrotreatment of fast pyrolysis liquids in batch and continuous set-ups using a bimetallic Ni-Cu catalyst with a high metal content, Catal. Sci. Technol. 6 (2016) 5899–5915.

[34] N. Navidi, J.W. Thybaut, G.B. Marin, Experimental investigation of ethylene hydroformylation to propanal on rh and co based catalysts, Appl. Catal. A 469 (2014) 357–366.

[35] K. Van der Borght, K. Toch, V. Galvita, J. Thybaut, G. Marin, Information-driven catalyst design based on high-throughput intrinsic kinetics, Catal. Today 5 (2015) 1948.

[36] R.J. Berger, E.H. Stitt, G.B. Marin, F. Kapteijn, J.A. Moulijn, Eurokin: chemical reaction kinetics in practice, CatTech 5 (2001) 30–60.

[37] D.E. Mears, Diagnostic criteria for heat transport limitations in fixed bed reactors, J. Catal. 20 (1971) 127–131.

[38] W. Dietz, Response factors for gas chromatographic analyses, J. Chromatogr. Sci. 5 (1967) 68–71.

[39] P.N. Brown, A.C. Hindmarsh, L.R. Petzold, Using Krylov methods in the solution of large-scale differential-algebraic systems, SIAM J. Sci. Comput. 15 (1994) 1467–1488.

[40] H. Rosenbrock, An automatic method for finding the greatest or least value of a function, Comput. J. 3 (1960) 175–184.

[41] D.W. Marquardt, An algorithm for least-squares estimation of nonlinear parameters, J. Soc. For. Ind. Appl. Math. 11 (1963) 431–441.

[42] J.A. Dumesic, D.F. Rudd, L.M. Aparicio, J.E. Rekoske, A.A. Trevino, The Microkinetics of Heterogeneous Catalysis, American Chemical Society, Washington, DC, 1993.

[43] K. Toch, J.W. Thybaut, G.B. Marin, A systematic methodology for kinetic modeling of chemical reactions applied to n-hexane hydroisomerization, AlChE J. 61 (2015) 880–892.

[44] T. Rajkhowa, G.B. Marin, J.W. Thybaut, A comprehensive kinetic model for cu catalyzed liquid phase glycerol hydrogenolysis, Appl. Catal. B: Environ. 205 (2017) 469–480.

[45] T. Yokoyama, N. Yamagata, Hydrogenation of carboxylic acids to the corresponding aldehydes, Appl. Catal. A 221 (2001) 227–239.

[46] N.A. Bhore, M.T. Klein, K.B. Bischoff, The delplot technique: a new method for reaction pathway analysis, Ind. Eng. Chem. Res. 29 (1990) 313–316.

[47] M.A. Alotaibi, E.F. Kozhevnikova, I.V. Kozhevnikov, Deoxygenation of propionic acid on heteropoly acid and bifunctional metal-loaded heteropoly acid catalysts: Reaction pathways and turnover rates, Appl. Catal. A 447–448 (2012) 32–40.

[48] J. Lu, S. Behtash, A. Heyden, Propanoic theoretical investigation of the reaction mechanism of the decarboxylation and decarbonylation of acid on pd(111) model surfaces, J. Phys. Chem. C 116 (2012) 14328–14341.

[49] J. Lu, M. Faheem, S. Behtash, A. Heyden, Theoretical investigation of the decarboxylation and decarbonylation mechanism of propanoic acid over a ru(0 0 0 1) model surface, J. Catal. 324 (2015) 14–24.

[50] Y.K. Lugo-José, S. Behtash, M. Nicholson, J.R. Monnier, A. Heyden, C.T. Williams, Unraveling the mechanism of propanoic acid hydrodeoxygenation on palladium using deuterium kinetic isotope effects, J. Mol. Catal. A Chem. 406 (2015) 85–93.

[51] L. Chen, Y. Zhu, H. Zheng, C. Zhang, B. Zhang, Y. Li, Aqueous-phase hydrodeoxygenation of carboxylic acids to alcohols or alkanes over supported ru catalysts, J. Mol. Catal. A Chem. 351 (2011) 217–227.

[52] L. Chen, Y. Zhu, H. Zheng, C. Zhang, Y. Li, Aqueous-phase hydrodeoxygenation of propanoic acid over the Ru/ZrO2 and Ru–Mo/ZrO2 catalysts, Appl. Catal. A: Gen. 411–412 (2012) 95–104.

[53] Y.K. Lugo-José, J.R. Monnier, C.T. Williams, Gas-phase, catalytic hydrodeoxygenation of propanoic acid, over supported group VIII noble metals: Metal and support effects, Appl. Catal. A 469 (2014) 410–418.

[54] G.W. Huber, J.A. Dumesic, An overview of aqueous-phase catalytic processes for production of hydrogen and alkanes in a biorefinery, Catal. Today 111 (2006) 119–132.

[55] M. Mavrikakis, M.A. Barteau, Oxygenate reaction pathways on transition metal surfaces, J. Mol. Catal. A Chem. 131 (1998) 135–147.

[56] J.L. Davis, M.A. Barteau, Decarbonylation and decomposition pathways of alcohol's on Pd(111), Surf. Sci. 187 (1987) 387–406.

[57] J.L. Davis, M.A. Barteau, Spectroscopic identification of alkoxide, aldehyde, and acyl intermediates in alcohol decomposition on pd(111), Surf. Sci. 235 (1990) 235–248.

[58] M. Myint, Y. Yan, J.G. Chen, Reaction pathways of propanal and 1- on Fe/Ni(111) and Cu/Ni(111) bimetallic surfaces, J. Phys. Chem. C 118 (2014) 11340–11349.

[59] L.E. Murillo, J.G. Chen, Adsorption and reaction of propanal, 2-propenol and 1-propanol on Ni/Pt(111) bimetallic surfaces, Surf. Sci. 602 (2008) 2412–2420.

[60] B. Peng, C. Zhao, I. Mejía-Centeno, G.A. Fuentes, A. Jentys, J.A. Lercher, Comparison of kinetics and reaction pathways for hydrodeoxygenation of C3 alcohols on Pt/Al2O3, Catal. Today 183 (2012) 3–9.

[61] H. Habazaki, M. Yamasaki, B.-P. Zhang, A. Kawashima, S. Kohno, T. Takai, K. Hashimoto, Co-methanation of carbon monoxide and carbon dioxide on supported nickel and cobalt catalysts prepared from amorphous alloys, Appl. Catal. A 172 (1998) 131–140.

[62] J. Liu, C. Li, F. Wang, S. He, H. Chen, Y. Zhao, M. Wei, D.G. Evans, X. Duan, Enhanced low-temperature activity of CO2 methanation over highly-dispersed ni/TiO2 catalyst, Catal. Sci. Technol. 3 (2013) 2627–2633.

[63] M. Cruz-Díaz, C. Buchaly, P. Kreis, E.S. Pérez-Cisneros, R. Lobo-Oehmichen, A. Górak, Synthesis of n-propyl propionate in a pilot-plant reactive distillation column: Experimental study and simulation, Comput. Chem. Eng. 39 (2012) 118–128.

[64] J. Wildschut, M. Iqbal, F.H. Mahfud, I.M. Cabrera, R.H. Venderbosch, H.J. Heeres, Insights in the hydrotreatment of fast pyrolysis oil using a ruthenium on carbon catalyst, Energy Environ. Sci. 3 (2010) 962–970.

[65] O. Deutschmann, Modeling and Simulation of Heterogeneous Catalytic Reactions: from the Molecular Process to the Technical System, John Wiley & Sons, Weinheim, 2011.

[66] V. Pallassana, M. Neurock, Reaction paths in the hydrogenolysis of acetic acid to ethanol over Pd(111), Re(0001), and PdRe alloys, J. Catal. 209 (2002) 289–305.

[67] J. Lu, S. Behtash, M. Faheem, A. Heyden, Microkinetic modeling of the decarboxylation and decarbonylation of propanoic acid over pd(111) model surfaces based on parameters obtained from first principles, J. Catal. 305 (2013) 56–66.

[68] V.M. Mello, G.P.A.G. Pousa, M.S.C. Pereira, I.M. Dias, P.A.Z. Suarez, Metal oxides as heterogeneous catalysts for esterification of fatty acids obtained from soybean oil, Fuel Process. Technol. 92 (2011) 53–57.

[69] I. Alstrup, On the kinetics of co methanation on nickel surfaces, J. Catal. 151 (1995) 216–225.

[70] Y. Chen, D.J. Miller, J.E. Jackson, Kinetics of aqueous-phase hydrogenation of organic acids and their mixtures over carbon supported ruthenium catalyst, Ind. Eng. Chem. Res. 46 (2007) 3334–3340.

[71] E. Licht, Y. Schächter, H. Pines, A comparative study of the reactions of alcohols over nickel-silica, silica-alumina, and nickel-silica-alumina catalysts in the presence of hydrogen, J. Catal. 38 (1975) 423–429.

[72] X. Wang, R.Y. Saleh, U.S. Ozkan, Reaction network of aldehyde hydrogenation over sulfided ni–mo/Al2O3 catalysts, J. Catal. 231 (2005) 20–32.

[73] J. Happel, I. Suzuki, P. Kokayeff, V. Fthenakis, Multiple isotope tracing of methanation over nickel catalyst, J. Catal. 65 (1980) 59–77.

[74] F. Koschany, D. Schlereth, O. Hinrichsen, On the kinetics of the methanation of carbon dioxide on coprecipitated NiAl(O)x, Appl. Catal. B: Environ. 181 (2016) 504–516.

[75] J. Kopyscinski, T.J. Schildhauer, F. Vogel, S.M.A. Biollaz, A. Wokaun, Applying spatially resolved concentration and temperature measurements in a catalytic plate reactor for the kinetic study of CO methanation, J. Catal. 271 (2010) 262–279.

[76] F.R. Abreu, M.B. Alves, C.C.S. Macêdo, L.F. Zara, P.A.Z. Suarez, New multi-phase catalytic systems based on tin compounds active for vegetable oil transesterificaton reaction, J. Mol. Catal. A Chem. 227 (2005) 263–267.

[77] S. Smeds, D. Murzin, T. Salmi, Kinetics of ethylbenzene hydrogenation on ni/Al2O3, Appl. Catal. A 125 (1995) 271–291.

[78] J.W. Thybaut, M. Saeys, G.B. Marin, Hydrogenation kinetics of toluene on Pt/ZSM-22, Chem. Eng. J. 90 (2002) 117–129.

[79] E.O. Odebunmi, D.F. Ollis, Catalytic hydrodeoxygenation, J. Catal. 80 (1983) 56–64.

[80] L. Nie, D.E. Resasco, Kinetics and mechanism of m-cresol hydrodeoxygenation on a Pt/SiO2 catalyst, J. Catal. 317 (2014) 22–29.

[81] A.A. Taimoor, I. Pitault, Kinetics of toluene hydrogenation—integrating a dynamic approach regarding catalyst activity, React. Kinet. Mech. Catal. 102 (2011) 263–282.

[82] L. Lozano, G.B. Marin, J.W. Thybaut, Analytical rate expressions accounting for the elementary steps in benzene hydrogenation on Pt, Ind. Eng. Chem. Res. 56 (2017) 12953–12962.

[83] P. Atkin, J. de Paula, Atkins' Physical Chemistry, WH Freeman and Company Books, 2006, pp. 747–755.

[84] T. Bera, J.W. Thybaut, G.B. Marin, Single-event microkinetics of aromatics hydrogenation on Pt/H-ZSM22, Ind. Eng. Chem. Res. 50 (2011) 12933–12945.

[85] W. Yin, R.H. Venderbosch, S. He, M.V. Bykova, S.A. Khromova, V.A. Yakovlev, H.J. Heeres, Mono-, bi-, and tri-metallic Ni-based catalysts for the catalytic hydrotreatment of pyrolysis liquids, Biomass Convers. Biorefinery 7 (2017) 361–376.